Biophysical Journal, Volume 98

Supporting Material

Salt dependent folding energy landscape of RNA three-way junction

Gengsheng Chen, Zhi-Jie Tan, and Shi-Jie Chen

Supporting Material for "Salt dependent folding energy landscape of RNA three-way junction"

Gengsheng Chen, Zhi-Jie Tan[†], and Shi-Jie Chen[*]
Department of Physics and Astronomy and
Department of Biochemistry
University of Missouri
Columbia, MO 65211

---

[*] Author to whom correspondence should be addressed: E-mail: chenshi@missouri.edu
[†] Present address: Department of Physics , Wuhan University, Wuhan, P.R.China 430072.
E-mail:zjtan@whu.edu.cn.

I. Structural model for three-way junction

We use the grooved primitive model (1) to model the A-RNA helix. In the grooved primitive model, each base pair in the helix is represented by five spheres: one central large sphere with radius 3.9 Å, two phosphate spheres with radii 2.1 Å, and two neutral spheres with radii 2.1 Å. For the canonical A-RNA, the coordinates of phosphate spheres (ρ_i^s, θ_i^s, z_i^s) are given by the canonical coordinates from x-ray measurements (2): $\rho_i^s = 8.8$(Å); $\theta_i^s = \theta_0^s + i\,32.73°$; and $z_i^s = z_0^s + i\,2.81$(Å), where $s = 1, 2$ denotes the two strands and $i = 1, 2, ...N$ denotes the nucleotides on each strand. The parameters (θ_0^s, z_0^s) for the initial positions are (0°, 0 Å) for the first strand and (153.6°, 1.88 Å) for the second strand, respectively. The neutral spheres have the same angular coordinates except they have the smaller radial coordinates 5.8 Å. The centers of the central large spheres are on the axis of RNA helix. Each phosphate sphere carries a point elementary charge $-q$ (electronic charge) at its center.

Using the above grooved primitive model, we can model the open (Y) and the folded (y) structures using parameters d_Y and d_y, see Fig. 7. In order for the different helical stems not to bump into each other, we require that $d_Y \gtrsim a$ and $d_y \gtrsim a + a\cos 60°$ (Figs. 7 A and B), where a (= 11 Å) is the radius of the helix. To generate the ensemble of conformations in the folding process, we chose a line passing through point A (Figs. 7 C, D and E) and perpendicular to the three-way junction plane as the rotate axis. We allow the 18-bp helix to rotate in the plane about this axis. Here, A is the middle point between corners B and C (Fig. 7 E). We use BC = $2b$ = 4.2 Å for the distance between the coaxially-stacking 18-bp and 15-bp stems. This distance is the average for the distance between nearest neighbors (2.8 Å) and the next nearest neighbors (5.6 Å) for the adjacent base pairs in an A-form helix. The distance is close to a previous theoretical prediction (3). Figs. 7 C, D and E show the rotation from the folded state to the open state. The folded structure parameters $d_y = ED = DF$, here $DF = BD + BF = a + b/(\tan 30°) \sim 15$ Å (Fig. 7 C). We slightly move point A so that DF in the open state is exactly 15 Å. We also use d_y = 17 Å, so the distances between the ends of the 15-bp stem and the 18-bp stem are equal to the experimentally measured donor-acceptor distances for the folded state and the open state. During the rotation of the 18-bp helix, we also radially and uniformly move the 15-bp helix in each step so that the helical stems do not bump into each other.

II. Parameter sets and details of numerical computation

We assume that Na^+ and Mg^{2+} ions are hydrated and have radii of 3.5 Å and 4.5 Å, respectively. In the test calculations for the ion size effect, we also use divalent ions of radii 3.5 Å and 5.5 Å. The dielectric constant is assumed to be 20 for the helix interior and 78 (of bulk water at 25 °C) elsewhere in the solution (4). Both the TBI and the PB calculations require numerical solution of the nonlinear PB. A thin layer of the thickness of one cation radius is added to the molecular surface to account for the excluded volume layer of the cations. We also use the three-step focusing process to obtain the detailed ion distribution near the molecules (5). The grid size of the first run depends on the salt concentration used. Generally, we keep it larger than four times of the Debye length, and the resolution of the first run varies with the grid size in order to make the iterative process computationally feasible (1, 4, 6, 7). The grid size (L_x, L_y, L_z) for the second and third runs are kept at (255, 204, 204) and (170, 119, 119) respectively, and the corresponding resolutions are 1.7 Å and 0.85 Å per grid, respectively. Correspondingly, the numbers of the grid points are 150×121×121 and 200×141×141 for the second and third runs. Our results are robust as tested against different grid sizes.

III. Calculations with the TBI theory

The computations with the TBI theory involve the following three steps (1, 4, 6, 7):

Step one.

For a given conformation of the three-way junction immersed in salt solution, we solve the nonlinear Poisson-Boltzmann equation (PB) to obtain the ion distribution $c(r)$. From $c(r)$ we determine the tightly bound region, which is defined as the region where the Coulombic correlation between the ions is strong, or the ions are so crowded that they start to bump into each other (1). The tightly bound region is usually a thin layer around RNA. We use PB to treat the rest (weakly correlated) ions.

Step two.

For an N-nt nucleic acid helix, we divide the tightly bound region into N cells, each around a phosphate. To account for the dielectric discontinuity at the RNA/solvent interface, we use generalized Born model (GB) to calculate the Coulomb interactions u_{ii} for charges in the same cell i and u_{ij} for charges in different cells i and j:

$$u_{ij} = u_{ij}^{pol} + u_{ij}^{0}, \tag{1}$$

$$u_{ij}^{pol} = -(\frac{1}{\epsilon_p} - \frac{1}{\epsilon_w})\frac{q_i q_j}{\sqrt{d_{ij}^2 + \alpha_i \alpha_j exp(-d_{ij}^2/(4\alpha_i \alpha_j))}} \tag{2}$$

$$u_{ij}^{0} = \frac{1}{\epsilon_p}\frac{q_i q_j}{d_{ij}} \tag{3}$$

where ϵ_p and ϵ_w are the dielectric constants of RNA helix interior and solvent, respectively; u_{ij}^{pol} is the polarization energy; and u_{ij}^{0} is the Coulombic interaction energy in the uniform medium of dielectric constant ϵ_p. The value d_{ij} is the distance between the two charges. The values α_i and α_j are the Born radii for the two charges q_i and q_j (4).

By averaging u_{ii} and u_{ij} over all the possible positions of the tightly bound ions inside the respective tightly bound cells, we compute the pairwise potential of mean force (PMF) $\Phi_1(i)$ and $\Phi_2(i, j)$. In the calculations for $\Phi_1(i)$ and $\Phi_2(i, j)$, the excluded volume effect between ions and between ions and the RNA are accounted for by a Lennard-Jones potential:

$V = (r/r_0)^{-12} - 2\,(r/r_0)^{-6} + 1, \quad$ for $r < r_0$

$V = 0, \quad$ for $r > r_0$

where r is the distance between the centers of the spheres that represent the ions and the charged/neutral groups of the RNA, r_0 is the sum of the radii for the two spheres. The calculated potentials of mean force are tabulated and stored for the calculations of partition function.

We also use the GB model to compute the Born energy $\Phi_0(i)$ for charges inside the ith tightly bound cell, which is calculated from an averaging of the self-energies of the phosphate i and of the ion over all the possible positions of the ion (4).

Step three.

We discretize the ion distribution according to the number of ions in each cell. A given distribution of the tightly bound ions is called a binding mode. We enumerate all the possible binding modes. For each mode, we calculate ΔG_b, ΔG_d and ΔG_b^{pol}:

$\Delta G_b = \sum_i \Phi_1(i) + \sum_{ij} \Phi_2(ij)$;
$\Delta G_b^{pol} = \sum_i \Phi_0(i)$;
$\Delta G_d = \frac{1}{2} \int \sum_\alpha c_\alpha(r) z_\alpha e[\psi(r) + \psi'(r)] d^3r + k_B T \times \int \sum_\alpha [c_\alpha(r) \ln \frac{c_\alpha(r)}{c_\alpha(0)} - c_\alpha(r) + c_\alpha(0)] d^3r$,
where the first and second integrals in ΔG_d correspond to the enthalpic and entropic parts of the free energy, respectively. The value $\psi'(r)$ is the electrostatic potential for the system without the diffusive salt ions.

Summation over the binding modes gives the total partition function Z, from which we can calculate the electrostatic free energy. The computational efficiency of the TBI model is limited by the enumeration of the binding modes, which scales with the number of nucleotides N as 2^N (for multivalent ions). Therefore, an exhaustive enumeration for all modes is extremely computationally expensive. In our previous study (8), we developed an efficient algorithm by including the low-energy modes exactly while sampling the high-energy modes using Monte Carlo method.

IV Coulomb correlation vs. excluded volume correlation

To test the importance of the excluded volume correlation vs. Coulomb correlation between the ions, we turn off the excluded volume effect in the TBI model. To switch off ion-ion excluded volume correlation, we set $V = 0$ for both $r < r_0$ and $r > r_0$ in the Lennard-Jones potential (see **Supplementary Material III**) and ignore the effect of ion-ion volume exclusion for the tightly bound ions in the configurational integral in Eq. 6.

V. The sensitity of the electrostatic free eenrgy to the non-planarity of the stems

To test the sensitivity of the electrostatic free energy to the non-planarity of the three helix stems, we retain the symmetry of the three-stem structure and rotate the helix stems off-plane with different angles (see Fig. S1). Using the different structures in Fig. S1 as the unfolded state, we find that small non-planarity does not cause significant changes to the predicted folding stability ΔG (see Fig. S2).

VI. The sensitivity of the electrostatic free energy to the orientation between the 15-bp and 8-bp helices

Following the experimental setup (the 8-bp helix is attached to a glass surface by a biotin moiety), we rotate the 15-bp helix slightly while fixing the other helices in order to vary the orientation between the 15-bp and 8-bp helices for the unfolded state. For the folded state, we use the structure as shown in the Supporting Material I. We calculate the electrostatic folding free energy to test the sensitivity to the orientation between 15-bp and 8-bp stems. We find that the electrostatic folding free energy is quite robust against small variations of orientation between 15-bp and 8-bp helix (see Fig. S3).

VII. Populational distribution of the different conformations

To test the validity of the two-state model for the ion concentrations used in the experiment, we investigate the probability(P) distribution of the different conformations for different ion concentrations. Here, $P = \mathrm{e}^{-\Delta G/k_B T} / \sum_i \mathrm{e}^{-\Delta G_i/k_B T}$ with $\Delta G = G(\theta) - G_{min}$, where G($\theta$) is the free energy landscape for different θ and G_{min} is the minimal free energy on the free energy landscape for the given ion concentration. As shown in Fig. S4, when the ion concentration are very low (Na^+=0.05 M or Mg^{2+}=0.000001 M), the maximally extended state is the most populous state. For high ion

concentrations (e.g. 1M Na^{+} or 0.001M Mg^{2+}), although the maximally extended (unfolded) state is still (weakly) favored electrostatically, the co-axial stacking force would stabilize the folded state so that the population is dominated by the folded state. Fig. S4 shows that for the ion concentrations used in the experiment (see Fig. 3S), the two-state model is a valid model.

References

[1] Tan, Z.J., and S.J. Chen. 2005. Electrostatic correlations and fluctuations for ion binding to a finite length polyelectrolyte. *J. Chem. Phys.* 122:044903.

[2] Tan, Z.J., and S.J. Chen. 2007. RNA helix stability in mixed Na^+/Mg^{2+} solution. *Biophys. J.* 92:3615-3632.

[3] Tyagi,R., and D.H. Mathews. 2007. Predicting helical coaxial stacking in RNA multibranch loops. *RNA.* 13:939-951.

[4] Tan, Z.J., and S.J. Chen. 2008. Electrostatic free energy landscape for DNA helix bending. *Biophys. J.* 94:3137-3149.

[5] Chen, S. W., and B. Honig. 1997. Monovalent and Divalent Salt Effects on Electrostatic Free Energies Defined by the Nonlinear Poisson-Boltzmann Equation: Application to DNA Reactions. *J. Phys. Chem. B.* 101:9113-9118.

[6] Montoro, J. C. G., and J. L. F. Abascal. 1995. Ionic distribution around simple DNA models. I. Cylindrically averaged properties. *J. Chem. Phys.* 103:8273-8284.

[7] Nikulin, A., A. Serganov, E. Ennifar, S. Tishchenko, N. Nevskaya, W. Shepard, C. Portier, M. Garber, B. Ehresmann, C. Ehresmann, S. Nikonov, and P. Dumas. 2000. Crystal structure of the S15-rRNA complex. *Nat.Struct.Biol.* 7: 273-277.

[8] Tan, Z.J., and S.J. Chen. 2006. Ion-mediated nucleic acid helix-helix interactions. *Biophys. J.* 91:518-536.

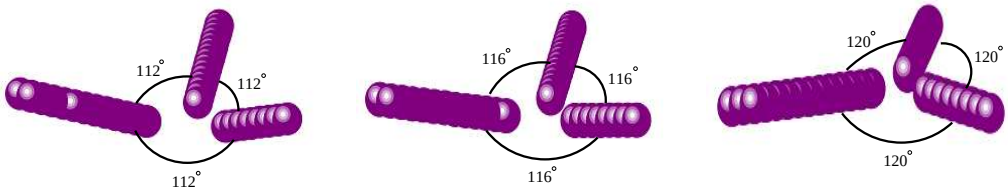

Figure S1: (Unfolded) structures used to test the validity of the co-planarity. From left to right, the inter-axis angles between each pair of helices are: 112° (non-planar), 116° (non-planar) and 120° (planar), respectively.

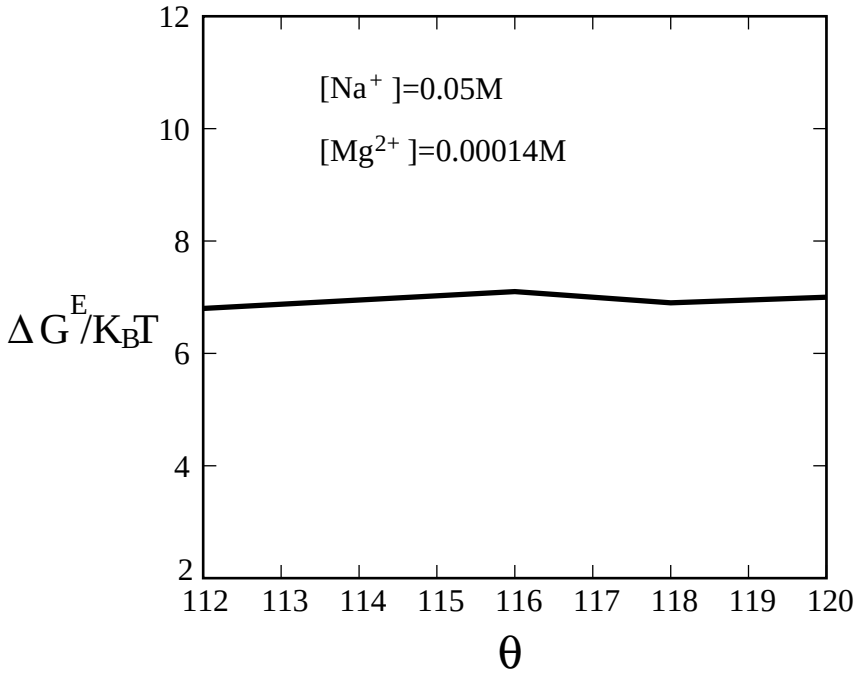

Figure S2: The electrostatic folding free energy ΔG in k_BT as a function of the inter-axis angles between each pair of helices. The inter-axis angles range from 112° to 120°.

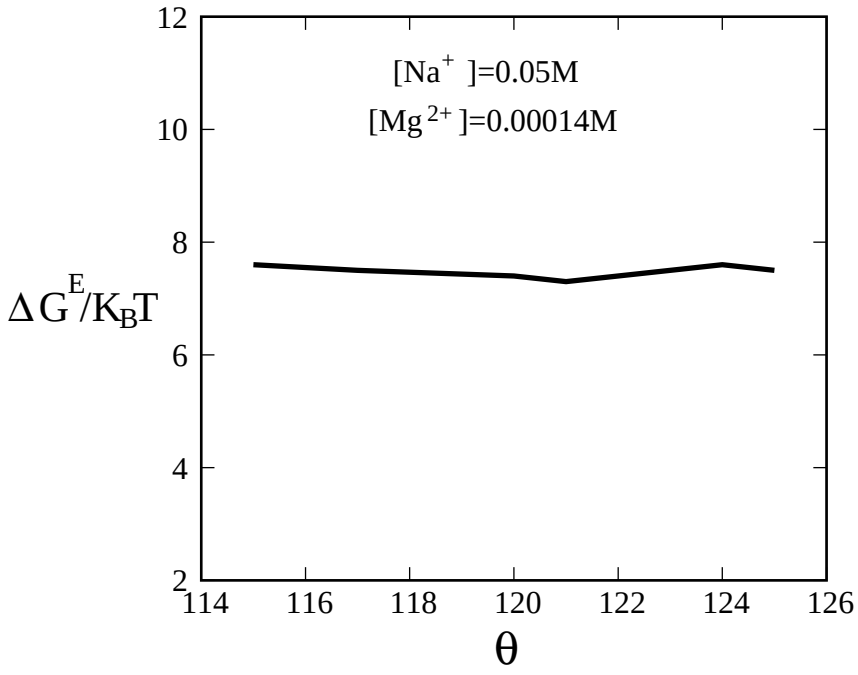

Figure S3: The electrostatic folding free energy ΔG in k_BT as a function of inter-axis angles between the 8-bp helix and the 15-bp helix. The inter-axis angles range from 115° to 125°.

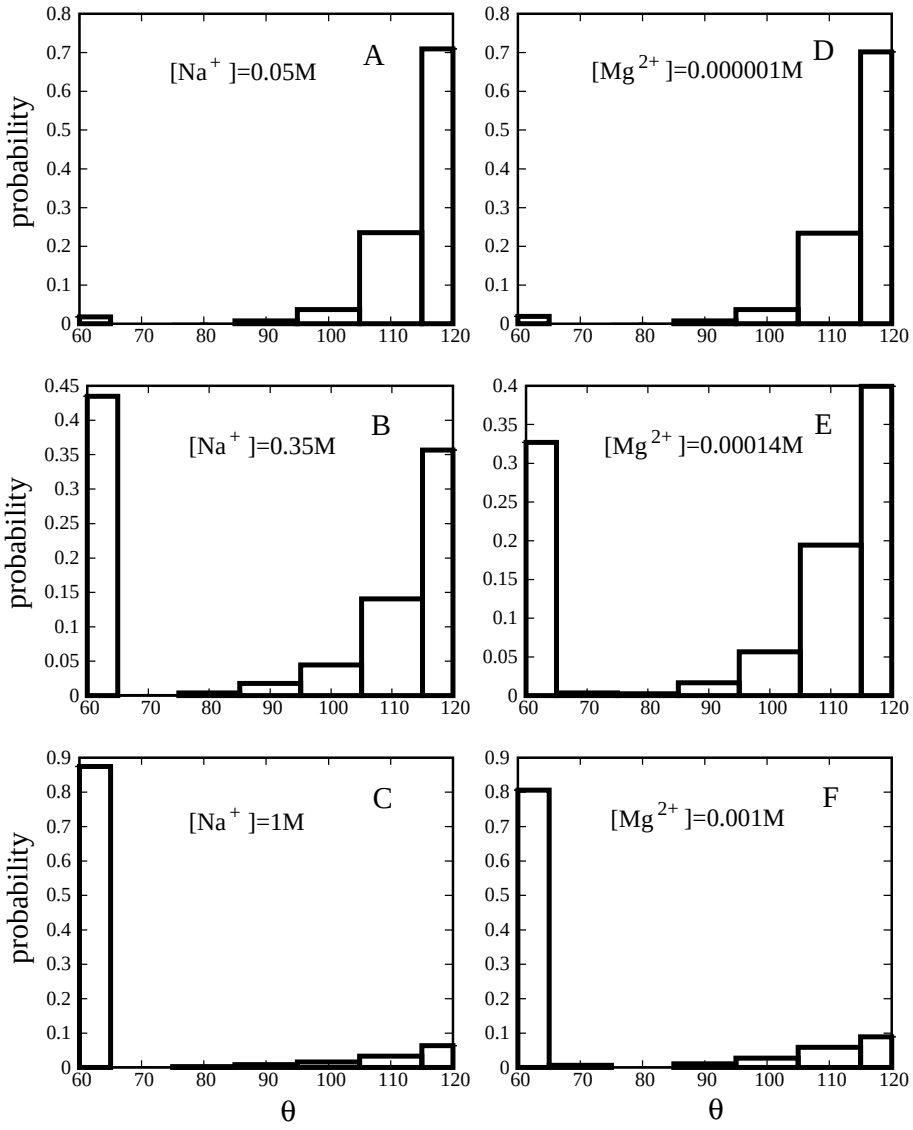

Figure S4: The fractional population of different states for different Na^+ and Mg^{2+} concentrations. The x-axis (θ) is the inter-axis angles between the 18-bp helix and the 15-bp helix. The y-axis is the probability distributions of different states. For the folded state $\theta = 60°$, the non-electrostatic free energy (for the coaxial-stacking) is added to the free energy.